CERN–PPE / 94–204
9 December 1994

ELECTROMAGNETIC SECONDARIES IN THE DETECTION OF HIGH ENERGY MUONS

RD5 Collaboration

C. Albajar[13], M. Andlinger[24], A. Arefiev[14], C. Bacci[19], Gy.L. Bencze[5], R. Bergman[15], A. Bettini[16], A. Bizzeti[8], C. Brouwer[15], R. Cardarelli[18], P. Casoli[16], S. Centro[16], F. Ceradini[19], E. Choumilov[14], D. Chrisman[22], G. Ciapetti[17], C. Civinini[8], D. Cline[22], R. D'Alessandro[8], M. Della Negra[6], E. Dénes[5], A. Di Ciaccio[18], W. Dominik[25], H. Faissner[1], A. Ferrando[12], M.C. Fouz[12], F. Gasparini[16], P. Giacomelli[23], I. Golutvin[7], W. Gorn[23], M. Górski[25], V. Gratchev[3a], I. Gramenitsky[7], A. Hervé[6], A. Iglesias[6b], M. Juntunen[10], V. Karimäki[10], V. Karjavin[7], R. Kinnunen[9], A. Kluge[24], A.C. König[15], Y. Kolotaev[14], M. Konecki[25], J. Królikowski[25], R. Labner[24], F. Lacava[17], J.G. Layter[23], R. Lauhakangas[10], I. Lippi[16], C. Lyndon[11], A. Malinin[14], R. Martinelli[16], R. McNeil[11], A. Meneguzzo[16], M. Meschini[8], T. Moers[1], M. Mohammadi[20], P. Moissenz[7], A. Nisati[17], D. Orestano[17], K. Österberg[21], S. Otwinowski[22], E. Petrolo[17], M. Pimiä[10], V. Pojidaev[8], C.L.A. Pols[15], V. Polychronakos[3], L. Pontecorvo[17], P. Porth[24], E. Radermacher[6], B. Razen[1c], D. Rein[1], H. Reithler[1], R. Ribeiro[6], A. Rojkov[14], J.P. Saarikko[10], R. Santonico[18], P. Sartori[16], H. Schwarthoff[1], C. Seez[6d], S. Selunin[7], J. Shank[4], B.C. Shen[23], F. Szoncso[24], M. Szeptycka[25], V. Tcherniatine[3e], H. Teykal[1], H. Tolsma[2], H. Tuchscherer[1f], J. Tuominiemi[9], T. Tuuva[10], H. van der Graaf[2], A. Vanyashin[20e], S. Veneziano[17], M. Verzocchi[17], G. Vesztergombi[5], M. Voutilainen[10], H. Wagner[1], G. Walzel[24], S. Whitaker[4], T. Wijnen[15], G. Wrochna[6,25], C.-E. Wulz[24], L. Zanello[17], A. Zarubin[7] and P. Zotto[16g].

[1*]Aachen, [2]Amsterdam (NIKHEF-H), [3†]BNL, [4]Boston, [5‡]Budapest, [6]CERN, [7]Dubna (JINR), [8]Firenze, [9]Helsinki, [10]Helsinki (SEFT), [11]Louisiana, [12§]Madrid (CIEMAT), [13¶]Madrid (Univ. Autónoma), [14]Moscow (ITEP), [15]Nijmegen, [16]Padova, [17]Roma "La Sapienza", [18]Roma "Tor Vergata", [19]Roma "Terza Università", [20‖]SUNY - Stony Brook, [21]Turku, [22]UCLA, [23]UC Riverside, [24]Vienna (HEPHY), [25**]Warsaw

Abstract

The experiments at the planned 14 TeV proton-proton collider LHC will need a good identification and measurement of muons with energies of up to about 800 GeV. The production of electromagnetic secondaries by muons of energy from 10 to 300 GeV has been measured at the RD5 experiment at CERN using various detector types proposed for LHC experiments. It is demonstrated that the detectors can recognize the presence of individual hits from e.m. secondaries, and that the muon measurement would be seriously compromised if these hits are not suppressed.

Submitted to Z. Phys. C

---

[a] Permanent address: St. Petersburg Nuclear Physics Institute.
[b] Doctoral student from Univ. of Santiago de Compostela, Spain
[c] Now at KFA Jülich, Germany.
[d] Visitor from Imperial College, London, U.K.
[e] Visitor from Moscow Engineering Physics Institute, Moscow, Russia.
[f] Now at Univ. of Alabama, USA.
[g] Now at Dipartimento di Física del Politecnico, Milano, Italy.

[*] Supported by Deutsches Bundesministerium für Forschung und Technologie.
[†] Supported by DOE contract DE-AC02-76CH00016.
[‡] Supported by Hungarian grant OTKA 4389.
[§] Supported by CICYT grant AEN92-0829.
[¶] Supported by CICYT grant AEN94-1253-E.
[‖] Supported by Texas NRLC awards RGFY92-118 and RGF93-312A, and by DOE contract DE-FG02-92ER40697.
[**] Supported by Polish KBN grants 2-0422-91-01 and SPUB 206/93.

1 Introduction

In view of the needs of the experiments at the future 14 TeV high luminosity Large Hadron Collider (LHC), especially for the search of extremely rare events like the Higgs and SUSY particles, the use of a very demanding and robust large area muon detector is essential. Identification of muons in the multi–GeV energy range is based on their large penetration depth in massive absorbers. Their momentum is measured by a magnetic spectrometer, usually located upstream of the absorber. The RD5 Collaboration at CERN [1], formed to study topics related to muon detection at future hadron colliders, has recently published first results on the measurement of a potentially harmful background, the hadronic shower punchthrough in iron [2, 3]. For identification and measurement of muons, two new aspects will play an important rôle at the LHC:
The number of tracks in the 'central tracker' in front of the absorber is very large and there are frequently single particles or even jets near the muon. Therefore, to obtain an unambiguous matching between the track in the central tracker and in the muon chamber, a good stand alone measurement of position, direction and momentum in the muon chambers is essential.
The high energy of the muons, of up to several hundreds of GeV, leads to a significant production of electromagnetic secondaries (knock-on 'δ' electrons, bremsstrahlung and pair production) by the muons themselves. Ionization has a constant cross section in our energy range, while pair production and bremsstrahlung have a cross section rapidly growing with muon energy and dominate at energies above about 300 GeV [6]. Nuclear interaction, having a cross section one order of magnitude smaller than bremsstrahlung and pair production, can be neglected. This radiation of secondaries near the muon track may jeopardize the precision of the muon track measurement.
In a run with horizontal cosmics (average energy above 50 GeV) and a massive, finely grained chamber, one finds that 6.6% of the muons induced a large e.m. shower with E $>$ 1 GeV and an energy distribution proportional to about E^{-2} [7], in agreement with earlier data on cosmic rays. The energy dependence of the energy deposition in a calorimeter was recently measured for muon energies up to 1 TeV [8].
It is therefore important to study the production of electromagnetic secondaries by muons and its impact on muon detectors. Muon-induced secondaries were studied at RD5 with different geometries (various distances from the absorber) and with various detector types (Silicon Beam Telescope, Honeycomb Strip Chamber, Cathode Strip Chamber, Wall-Less Drift Chamber, Drift Tube with Bunch Crossing Capability, Resistive Plate Chamber). For a description of the experimental arrangement see [2, 3]. In chapter 2 we present a measurement, made with a silicon tracker, of the secondaries emerging from an iron absorber. The following sections address the question whether e.m. secondaries can be recognized at the level of one muon station (4–8 single layers in each projection), or even at the level of the individual layer of the large area muon chambers. In section 3 we discuss basic approaches to minimize the number of e.m. secondaries close to the muon track in the muon chambers. The impact of the presence of e.m. secondaries on the track reconstruction will largely depend on the fraction which remains unrecognized, and thus also on the details of the analysis. Although in the future the analysis tools will evolve further, we discuss in the last section an example of how the presence of secondaries affects the reconstructed track.

2 Experimental observation of induced e.m. particles

2.1 Electromagnetic secondaries in Silicon Detector

A dedicated study of high energy δ–rays and electromagnetic showers induced by high energy muons passing through dense materials has been performed during the 1992 and 1993 runs of the RD5 experiment, using a Silicon Beam Telescope (SiBT) placed behind a 30 cm thick iron absorber. The very good spatial and two-track resolution of the silicon microstrip detectors are used to distinguish the electron hits from the muon hits down to a distance of 100 μm.
The SiBT is composed of nine planes of 500 μm thick silicon microstrip detectors covering an area of 2.6$\times$5.8 cm^2 and equipped with analog readout electronics [10]. The strips have a pitch of 50 μm and are 2.6 cm long. Four of the nine planes measure the horizontal coordinate and the other five measure the vertical one. The planes are positioned at distances ranging from 5 to 50 cm from the edge of the iron absorber. The display of an event, where the muon track is accompanied by two

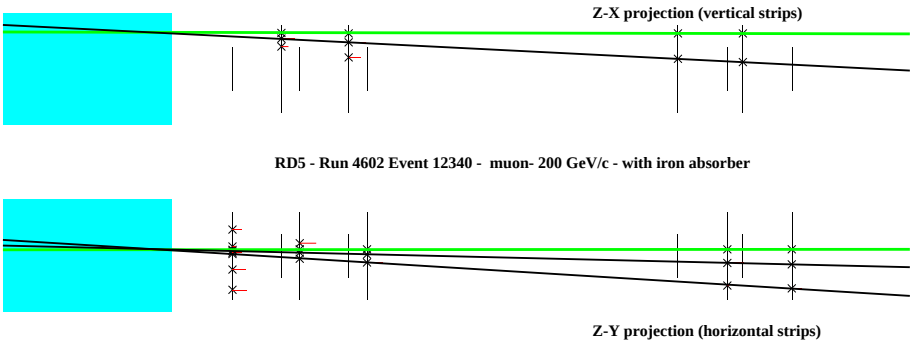

Figure 1: Display of one event in the SiBT, in which a 200 GeV/c muon (dotted track) has generated two electrons in the iron block, of which one is reconstructed in both projections.

energetic electrons traversing several planes of the telescope, is shown in Fig. 1.
Due to the absence of stereo layers no attempt has been made to reconstruct tracks in space and the two projections have been treated separately. In absence of a magnetic field the distribution of generated electrons is uniform in azimuth. Thus, on a statistical basis, it is possible to merge the data from the two projections even if for single events the angular acceptance is different.
Data were taken with a μ^- beam of 50, 100, 200 and 300 GeV/c momentum, both with and without the iron absorber in front of the silicon telescope. Data taken without the iron absorber are used to correct for the fraction of electrons generated in the silicon planes. The detector noise contribution is estimated using pedestal runs and is reduced well below the noise due to electrons generated in the silicon by a combined cut on the cluster size and on the signal to noise (S/N) ratio of each cluster: the average S/N ratio and cluster size for minimum ionizing particles are 30 and 2.5, respectively, whereas the electronic noise is characterized by low S/N ratio and by single strip clusters.
The first step of the analysis is to require the presence of a muon track reconstructed in the SiBT and confirmed in subsequent detectors. If more than one track is reconstructed in the silicon telescope, the one with the smallest deviation from the average beam direction is taken. In each plane with a hit linked to the muon track, we look for additional hits which satisfy the cuts on the cluster size and on the S/N ratio, and measure the distance of the center of the cluster from the muon track. At the same time we count the number of events which have additional hits on the silicon planes and measure their multiplicity. In Fig. 2 and in Table 1 we show the fraction of events which have at least one additional hit in a plane, at a distance from the muon hit between 100 μm and 2.5 cm (the lower limit being given by the two track resolution and the upper one by the detector size), as a function of the distance of the silicon plane from the iron absorber and for different beam energies.
The distributions show that the fraction of events with additional hits in the detectors increases with energy as expected, reaching a value of 12.7% for the nearest plane, for a muon momentum of 300 GeV/c. The decrease of the fraction of events with additional hits when moving away from the iron absorber is due both to the limited geometrical acceptance and to the absorption of electrons and photons in the 500 μm thick silicon planes. The dominating error is the uncertainty in the subtraction of the electronic noise, due to its fluctuations; other sources of errors, like the criteria used to define the muon track, are less important. Large acceptance corrections are needed in order to compare the data obtained with the SiBT with data taken with other detectors of larger acceptance. However the data obtained with the SiBT are useful, since for muon pattern recognition and for precise momentum measurement the most dangerous δ–rays are those emitted at small angles.
The data is compared with the results of a simulation program based on GEANT 3.21 [9]. In

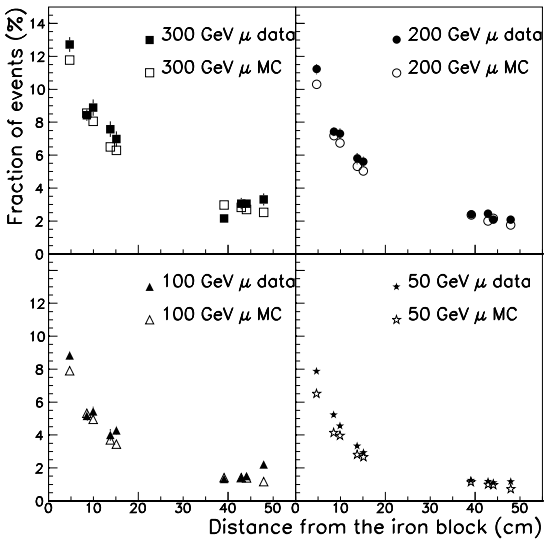

Figure 2: Fraction (%) of events in SiBT with at least 1 additional hit $\geq$100 μm apart from the muon track in the silicon planes, versus the distance of the detector plane from the iron absorber, for different beam energies.

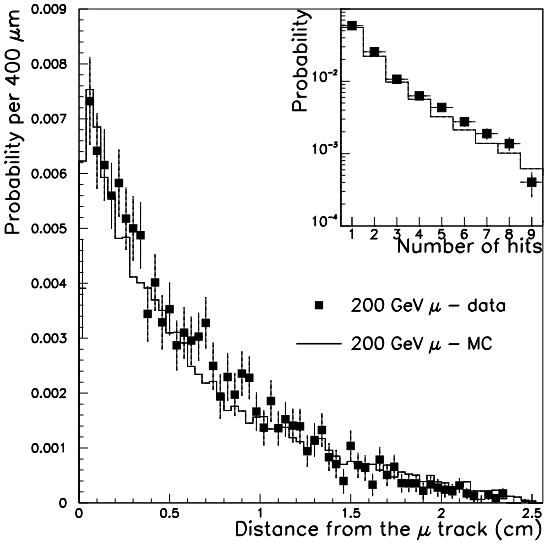

Figure 3: Distribution of the distance of additional hits in the SiBT due to showering induced by a muon in the iron, at 4.7 cm from the absorber. The insert shows the probability distribution of the number of additional hits.

the Monte Carlo simulation, the electrons and photons generated by a muon passing through dense material are traced until their kinetic energy falls below 10 keV. Electrons are explicitly generated and traced if their kinetic energy is above 70 keV, which corresponds to an average range of approximately 60 μm in silicon. The noise measured in pedestal runs is then added and the response of the readout chain is fully simulated. Simulated events are then reconstructed and analyzed with the same criteria used for the real data. The distributions for the fraction of additional hits in the silicon planes as a function of the distance from the iron absorber at different muon energies obtained with the simulation are included in Fig. 2 and are in good agreement with the experimental results.

Figure 3 shows (for a 200 GeV/c beam momentum and at the nearest detector plane) the distribution of the distance of additional hits from the muon track, comparing again the data and the simulation, after subtraction of the data taken without the iron absorber in front of the silicon telescope. The distribution of the number of additional hits in this silicon plane due to the electromagnetic interaction of the muons in the iron absorber is also shown.

The good intrinsic resolution of the silicon detectors allows to calculate the reduction of the number of muon hits spoiled by the presence of electrons that would be possible in other detectors with any given two hit resolution. Tables 2 and 3 show the fraction of events which have at least one additional hit within 5 and 2 mm, respectively. For a drift chamber, in half of the events the muon hit will be closer to the anode wire than the electron hit, hence providing nevertheless the correct muon hit measurement.

The data obtained with the SiBT show that the high energy δ–rays and electromagnetic showers accompanying high energy muons in dense materials can affect a sizeable fraction of the muon tracks above 100 GeV/c; the GEANT simulation agrees quite well with the data at different energies and at various distances from the iron absorber. Also, the distribution of the background hits around the muon track is well reproduced.

distance from the iron (cm)	muon momentum (GeV/c)			
	50	100	200	300
4.70	$7.88 \pm 0.20 \pm 0.25$	$8.83 \pm 0.27 \pm 0.25$	$11.21 \pm 0.30 \pm 0.25$	$12.72 \pm 0.46 \pm 0.25$
8.52	$5.22 \pm 0.18 \pm 0.31$	$5.16 \pm 0.26 \pm 0.31$	$7.42 \pm 0.27 \pm 0.31$	$8.43 \pm 0.35 \pm 0.31$
9.91	$4.55 \pm 0.22 \pm 0.59$	$5.43 \pm 0.30 \pm 0.59$	$7.30 \pm 0.32 \pm 0.59$	$8.89 \pm 0.50 \pm 0.59$
13.73	$3.34 \pm 0.18 \pm 0.42$	$4.01 \pm 0.35 \pm 0.42$	$5.82 \pm 0.37 \pm 0.42$	$7.58 \pm 0.47 \pm 0.42$
15.11	$2.94 \pm 0.20 \pm 0.64$	$4.29 \pm 0.27 \pm 0.64$	$5.61 \pm 0.30 \pm 0.64$	$6.97 \pm 0.46 \pm 0.64$
39.07	$1.25 \pm 0.12 \pm 0.49$	$1.33 \pm 0.14 \pm 0.49$	$2.41 \pm 0.16 \pm 0.49$	$2.16 \pm 0.21 \pm 0.49$
42.89	$1.18 \pm 0.13 \pm 0.59$	$1.41 \pm 0.19 \pm 0.59$	$2.44 \pm 0.22 \pm 0.59$	$3.06 \pm 0.34 \pm 0.59$
44.07	$1.11 \pm 0.13 \pm 0.42$	$1.51 \pm 0.17 \pm 0.42$	$2.11 \pm 0.18 \pm 0.42$	$3.05 \pm 0.24 \pm 0.42$
47.90	$1.17 \pm 0.14 \pm 0.48$	$2.22 \pm 0.20 \pm 0.48$	$2.07 \pm 0.22 \pm 0.48$	$3.31 \pm 0.37 \pm 0.48$

Table 1: Fraction (%) of events with at least one additional hit in each 2.6×5.8 cm^2 silicon detector plane as a function of the distance of the plane from the iron absorber, for different beam energies. The first error is statistical, the second represents the uncertainty in the subtraction of the electronic noise.

distance from the iron (cm)	muon momentum (GeV/c)			
	50	100	200	300
4.70	4.37 ± 0.23	5.60 ± 0.33	7.32 ± 0.37	8.53 ± 0.54
8.52	3.39 ± 0.21	3.27 ± 0.33	4.09 ± 0.34	5.23 ± 0.45
9.91	2.65 ± 0.28	3.22 ± 0.35	5.17 ± 0.38	5.34 ± 0.59
13.73	2.05 ± 0.20	2.65 ± 0.46	4.14 ± 0.52	5.39 ± 0.69
15.11	1.84 ± 0.23	2.50 ± 0.28	3.24 ± 0.32	3.47 ± 0.50
39.07	0.73 ± 0.13	1.09 ± 0.16	1.10 ± 0.17	1.10 ± 0.24
42.89	0.58 ± 0.15	0.90 ± 0.20	1.25 ± 0.24	2.13 ± 0.37
44.07	0.21 ± 0.15	0.80 ± 0.20	1.13 ± 0.21	1.51 ± 0.30
47.90	0.68 ± 0.16	1.23 ± 0.22	1.51 ± 0.24	1.76 ± 0.38

Table 2: Fraction (%) of events with at least one additional hit within 5 mm (in one projection) from the muon hit as a function of the distance of the detector plane from the iron absorber for different beam energies (statistical errors only).

distance from the iron (cm)	muon momentum (GeV/c)			
	50	100	200	300
4.70	2.48 ± 0.15	2.96 ± 0.21	3.73 ± 0.24	5.04 ± 0.37
8.52	1.54 ± 0.14	1.23 ± 0.24	2.07 ± 0.25	3.01 ± 0.33
9.91	1.44 ± 0.19	1.69 ± 0.23	2.55 ± 0.25	3.09 ± 0.39
13.73	0.92 ± 0.12	1.71 ± 0.29	2.34 ± 0.34	3.88 ± 0.45
15.11	0.70 ± 0.15	1.24 ± 0.17	1.69 ± 0.20	1.90 ± 0.32
39.07	0.38 ± 0.10	0.57 ± 0.11	0.52 ± 0.12	0.70 ± 0.16
42.89	0.46 ± 0.10	0.29 ± 0.13	0.65 ± 0.15	1.07 ± 0.25
44.07	0.25 ± 0.10	0.45 ± 0.13	0.48 ± 0.13	0.72 ± 0.19
47.90	0.39 ± 0.11	0.41 ± 0.14	0.77 ± 0.15	1.20 ± 0.25

Table 3: Fraction (%) of events with at least one additional hit within 2 mm (in one projection) from the muon hit as a function of the distance of the detector plane from the iron absorber for different beam energies (statistical errors only).

2.2 Electromagnetic secondaries in Honeycomb Strip Chamber

Honeycomb Strip Chambers (HSCs) [11] are position sensitive, gaseous detectors with hexagonally shaped proportional drift tubes. The chambers are made of layers of folded 75 μm thick polyester films which are glued together. These films are provided with copper cathode strips with an orientation perpendicular to the folds. An anode wire (30 μm W/Au) is strung in the center of each hexagonal cell. A two-dimensional readout is therefore obtained in a HSC for particles crossing a drift tube: one coordinate can be deduced from the drift time, and the second coordinate is derived from the induced charge distribution on the cathode strips. The HSCs for the present study have a single layer and cover an active area of 0.6×0.8 m^2. Each HSC has 192 strips with a pitch of 5.08 mm and 48 hexagonal cells with a wire pitch of 12.7 mm and an outer cell radius of 5.77 mm. A total of 25 HSCs are interleaved with stainless steel absorbers to form a Tracking Calorimeter (TRACAL) [12]. The chambers were positioned in the gaps of 22 mm average width. The absorber thickness is 40 mm (a quarter of an interaction length) between the first 13 HSCs and 80 mm in the rear section, amounting to about 84 radiation lengths in total.

The strip information for a typical muon event is shown in Fig. 4. A selection of strips carrying the largest charge (Q_{middle}) was made after calibration of the raw ADC data. The charge carried by its neighbour on each side was called Q_{left} and Q_{right} respectively. A threshold was applied to the sum of the three signals.

The observed distribution of the ratio Q_{right}/Q_{middle} versus Q_{left}/Q_{middle} (for a single layer) is plotted in Fig. 5. This distribution is expected from simulation to be lying within the range indicated by the solid lines in Fig. 5. The entries above the curve are indicative of a charge distribution wider than that expected for a single muon track. We attribute these entries to the superimposed charge distributions of a muon and one or more electrons created in the absorber by the primary muon. The probability for measuring, in one layer, an incident muon accompanied with one or more electrons is about 15% for 20 GeV/c incident muons and increases up to 25% for 300 GeV/c muon momentum. These percentages are obtained from the number of entries above the expected range, normalized to the total number of entries in the plot.

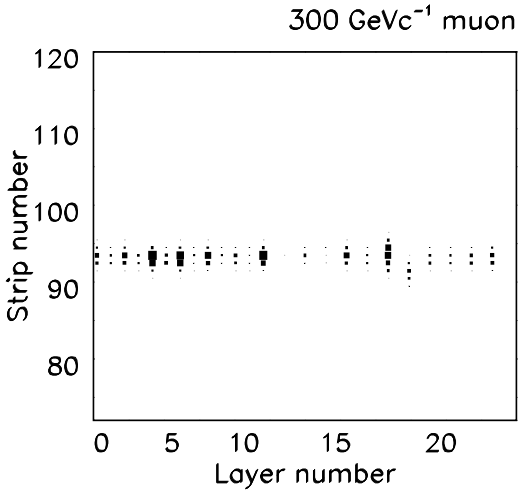

Figure 4: A typical muon track through TRACAL. The box size is proportional to the charge collected by the indicated strip.

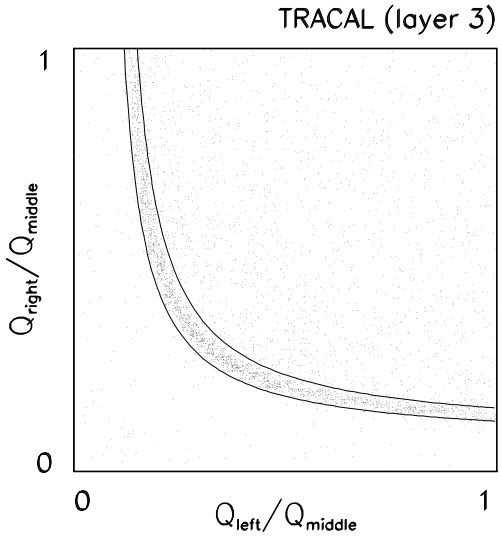

Figure 5: The ratio Q_{right}/Q_{middle} plotted against Q_{left}/Q_{middle} for a single-layer HSC in TRACAL. The entries above the expected range (solid lines) are clearly visible.

Confusing multi-track measurements can be recognized and a cut applied to remove events with

too broad charge distributions. Therefore, the strip information is a powerful tool for muon track reconstruction. The muon track shown in Fig. 4 reveals some typical shower contamination (layers 18 and 19). The height of the charge signals is usually larger for contaminated events, and the position of the center of gravity of the charge distribution is clearly off the incident track.

2.3 Electromagnetic secondaries in Cathode Strip Chamber

Muon induced e.m. secondaries were also studied with two Cathode Strip Chamber (CSC) prototypes [13, 14] consisting of 4 layers of 0.5×0.5 m^2. The chamber material amounts to 0.05 radiation length. The CSC is a multiwire proportional chamber with highly segmented cathodes in which the precise coordinate across the cathode strips is determined by computing the centroid of the charge induced on the strips. With a cathode strip readout pitch of 5 mm, a spatial resolution of about 40 μm at normal incidence is achieved. Anode wires with 2.5 mm pitch form a plane at 2.5 mm distance from the cathode planes. The short drift length provides good timing capability. The anode wires are OR-ed together to form 50 mm wide groups for a coarse measurement of the second coordinate. Secondaries produced inside the CSC and those produced in an absorber block placed upstream of the CSC were studied.

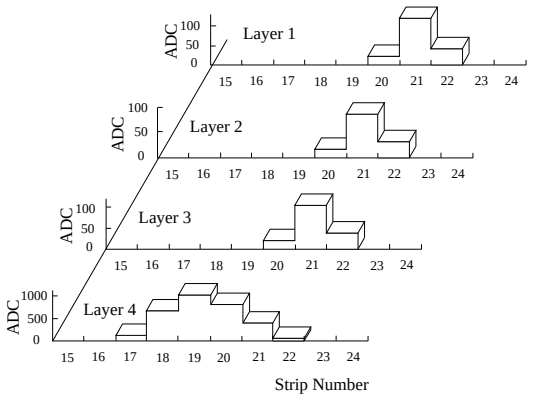

Figure 6: Display of a typical event in the CSC, with a single track reconstructed in the three upper layers. The charge distribution in the fourth layer (bottom) identifies it as an event with δ-electron production, since it is clearly wider and shifted w.r.t. the primary particle track.

Data from vertical cosmic rays obtained with the first prototype [13] were used to study the production of secondaries inside the CSC, i.e. with hits close to the muon track. The charge distribution (or cluster) in each layer typically consists of three strips with the largest charge (Q_{middle}) at the center and its neighbours on both sides with charges Q_{left} and Q_{right}. The 4 CSC layers allow to reconstruct a straight track in 3 layers and to measure the residual in the fourth layer, as exemplified by the event in Fig. 6. The study of the charge deposition in the fourth layer also allows the identification of the presence of δ-electrons. Tracks were selected in the following way: we required clusters of at least 3 strips in each of the 3 layers, and a straight line within a spatial window of ± 3 standard deviations of the chamber resolution. The distribution of the ratio Q_{right}/Q_{middle} versus Q_{left}/Q_{middle} in the fourth layer is shown in Fig. 7. The corresponding charge distribution measured in the 3 selected layers is confined to the region limited by the solid curves in Fig. 7. The events above the curve have a charge distribution wider than that measured with the criteria above for single tracks. These events were identified as a superposition of the charge distributions of a primary particle and of δ-electron(s) produced in the CSC.
The δ-electron production probability, obtained from the fraction of events outside the expected range for single tracks, in this scatter plot, is $11.8\% \pm 1.2\%$ per layer. The estimate of the fraction of δ-electrons confined to one layer is obtained from an analysis of the inner layers and amounts to $78.8\% \pm 12.3\%$ of the events with δ-electrons.

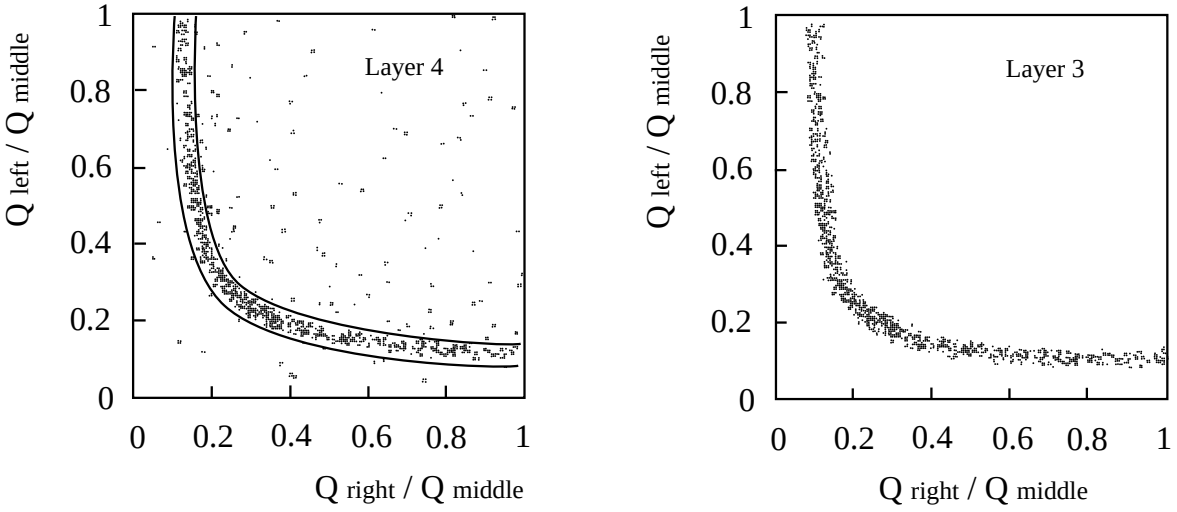

Figure 7: Scatter plot of the ratio Q_{left}/Q_{middle} versus Q_{right}/Q_{middle} in the CSC, for events with a single track reconstructed in three layers (labelled 1-3). As shown for layer 3 (right), the charges in these layers all lie within a narrow band. This band is also indicated in the distribution for the fourth layer (solid lines, left). Events above the expected range, in the fourth layer, are identified as a cosmic ray accompanied by δ-electron(s). The position sensing cathode strips have a readout pitch of 5 mm.

The effect of e.m. secondaries generated by high energy muons passing through dense material was studied in the RD5 setup with the second CSC prototype [14]. The dense material was a 40 cm block of copper placed 30 cm upstream of the chamber. The large sensitive area of the chamber allowed measurements of the secondaries at large distances from the muon track. These secondaries, which are predominately produced in the copper, do not compromise the position measurement but they might affect muon triggering.

Figure 8 shows the distribution of the number of hits per chamber layer, averaged over four layers. A hit was defined as a 5-strip charge cluster, where the strip with the largest charge (the middle strip) was above a threshold adjusted for each layer to give an efficiency of 95% for a muon. Additional hits were similarly found across all strips in a layer, excluding those belonging to the previous hits. The comparison of the data taken at 200 and 300 GeV/c shows that the rate of multi-hit ($\geq$3) events is about 20% larger for higher energy muons.

To study the presence of muon-induced secondary tracks, two additional requirements were applied: the strip with the largest charge in the cluster had to have a charge of 5σ above noise (i.e. to be $>$2 fC) and the total cluster charge had to be $>$10 fC. To resolve close tracks with overlapped clusters, we relied on the stability of the shape of the induced charge distribution from a single particle at normal (or nearly normal) incidence in the CSC. This shape was parametrized using the data. A hit was considered as two (overlapped) hits if its shape was better fitted by a 2-particle hypothesis. A 'track' was then defined as a set of four hits, one per layer (no pattern recognition performed) and '2-track' events were selected by requiring at least two hits in each of the four chamber layers.

The average separation between the first and the second hits found in the four layers is a measurement of the separation between the muon and the secondary track; it is distributed as shown in Fig.9. The maximum separation shown is 150 mm because of the geometrical acceptance. The solid line shows the prediction of a GEANT-3.21 based Monte Carlo simulation, which agrees well with the overall shape and rate of this distribution. The measured probability of observing a secondary e.m. track is (10.3$\pm$0.2)% for 200 GeV/c and (11.6$\pm$0.2)% for 300 GeV/c incident muons.

The same results were obtained when the analysis was repeated with the additional requirement

that only one track, as reconstructed in the upstream muon chambers, entered the copper block. This verified that the measured secondary hits were indeed caused by muon-induced secondaries and not by beam halo.

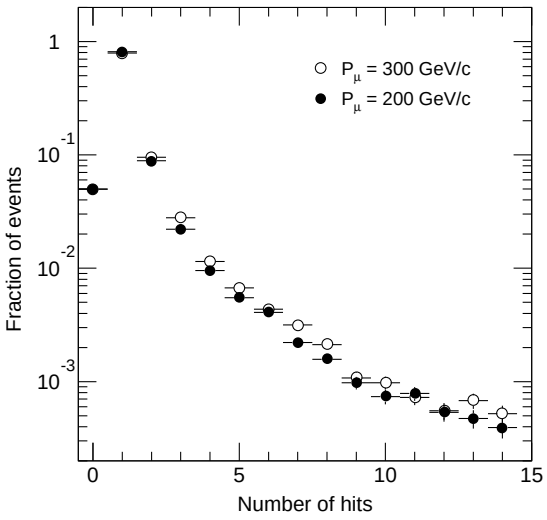

Figure 8: Distribution of number of hits per CSC layer for 200 GeV/c and 300 GeV/c incident muons.

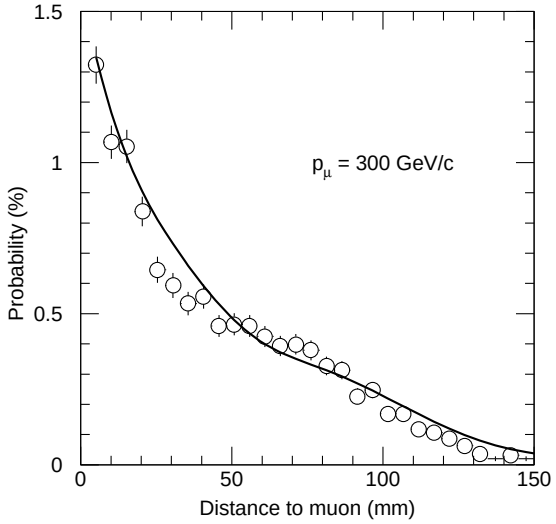

Figure 9: Comparison of GEANT Monte Carlo simulation (line) and measured (points) probability of secondary tracks vs. the distance from the muon for 300 GeV/c incident muons. 'Tracks' taken here as charge clusters in all 4 CSC layers.

2.4 Electromagnetic secondaries in Wall-Less Drift Chamber

The Wall-Less Drift Chamber (WLDC) [15] is a small-cell modular drift chamber with a maximum drift time of 110 ns. Groups of 16 cells with 14 mm width and separated by pairs of cathode wires form a multi-cell unit. The 46 wires of one multi-cell are housed between two conductive covers held at ground potential. The covers are cylindrically shaped around each wire and at 3.5 mm distance from them, to improve the field shaping and serve as collimator to avoid very late electrons along drift lines near the covers. A WLDC module consists of 10 drift chamber layers with 20 mm pitch to measure the track position and angle, and two layers of Resistive Plate Chambers (RPC) [17] with small square pads to assign the beam crossing and to resolve spatial ambiguities in the reconstruction. The present data were obtained with an aluminum chamber with 8 layers measuring one projection, exposed to cosmics and to a monoenergetic muon beam.

The presence of e.m. secondaries in the WLDC is recognized after the track reconstruction by observing the 'signed residuum', i.e. the distance between hit and reconstructed track. The residua are given a negative sign if the hit is nearer to the anode than the reconstructed track. With an average pulse length of 250 ns in the WLDC, a hit from a δ-electron passing the chamber nearer to the anode than the muon masks the muon hit. The distribution of the signed residua therefore shows an asymmetric tail (Fig. 10). The signed residua from the simulation (Fig. 11) show the same tail as those from the data. If no secondaries are produced, the distribution is symmetric, as also shown in Fig. 11. Hence the hits in the tail are indeed caused by δ-electrons and other secondaries. The fraction of *hits* with a residuum larger than 600 μm is 9% (taken from Fig. 10). The fraction of *tracks* with hits in the asymmetric tail is given in Table 4. The first column shows that about 71% of such 8-point tracks are undisturbed [16]. It should be noted that changes in the reconstruction

energy of muon		number of hits outside 3σ (8-hit tracks)			
		0	1	2	more than 2
10 GeV	data	73	10	9	9
	simulation	75	11	7	7
50 GeV	data	68	11	11	10
	simulation	72	12	8	8
100 GeV	data	71	10	8	10
	simulation	72	11	8	9
200 GeV	data	68	12	9	12
	simulation	71	10	8	10

Table 4: Fraction (%) of 8-hit tracks with n residua larger than 3σ of the single hit resolution for WLDC data and simulation.

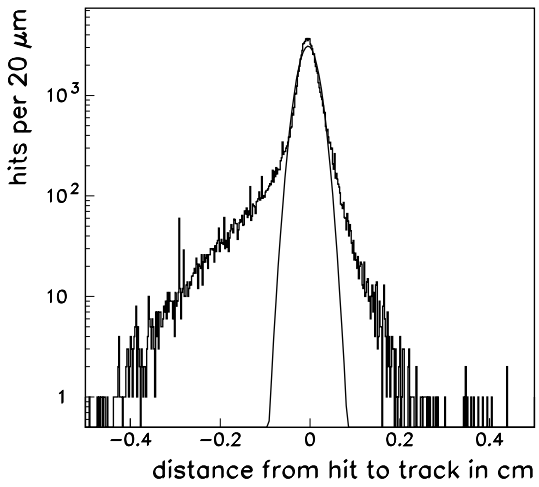

Figure 10: WLDC data (200 GeV muons): Signed residua of a reconstructed muon track, with logarithmic scale to show the asymmetry. The anode is on the left side. A fitted gaussian is also shown.

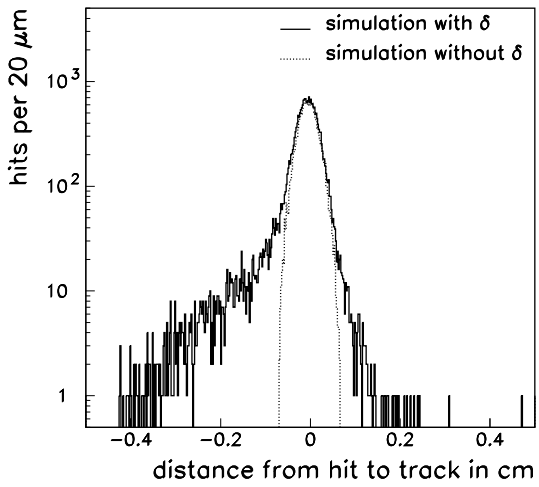

Figure 11: WLDC simulation (200 GeV muons): Signed residua of reconstructed tracks, with logarithmic scale to show the asymmetry. The solid line is the simulation including δ-electrons, the dotted line is the simulation without generation of secondaries.

algorithm modify the classification in 1, 2, and >2 hits outside 3σ, but the simulation reproduces this behaviour.

2.5 Electromagnetic secondaries in Drift Tubes with Bunch Crossing Capability

The Drift Tubes with Bunch Crossing Capability (DTBX) [18] are a drift chamber consisting of staggered plastic tubes which form drift cells of 38×10 mm^2 cross section. In a three layer array of drift tubes, assuming a linear space-time relationship, accurate wire positioning and accurate layers staggering, a particle crossing at normal incidence (Fig. 12a) originates in consecutive cells drift times that satisfy the relations $t_M = t_A + t_B$ and $t_M = t_B + t_C$ where t_M is the maximum possible drift time. If the track is inclined the relations are $t_M = t_D + t_E - \Delta t(\theta)$ and $t_M = t_E + t_F + \Delta t(\theta)$ as can be argued from Fig. 12b. The mean-timer sum $t_M = t_E + (t_D + t_F)/2$ is a constant and corrects for systematic errors coming from muon inclination.

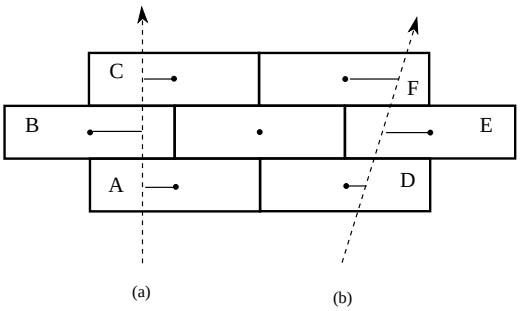

Figure 12: Principle of mean–timer operation.

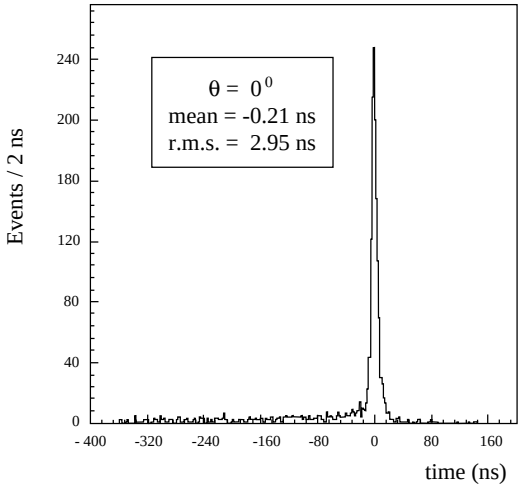

Figure 13: Time distribution of the mean–timer sum for a DTBX exposed to 200 GeV/c muons under normal incidence on the chamber.

A DTBX prototype was placed 50 cm downstream a shielding block and exposed to muon beams of 100, 200, 300 GeV/c momentum. The distribution of t_M for a typical triplet of tubes at normal beam incidence is shown in Fig. 13 where the time origin is set at the center of the peak. We can see that, apart from the expected peak due to ideal muons, there is a long tail towards negative values. This tail may have several causes: noise, electric field shaping, cross-talk, double beam tracks, and muon induced secondaries. Noise and cross-talk were found to be negligible, while cell uniformity was checked with a fine scanning through it.

It has been found that the affected events can be divided into two classes: single hits causing a wrong mean–timer measurement and events with hits in more than one cell per layer. We interpret the first class as soft δ–rays (affecting only one layer) and the second one as electromagnetic showers and penetrating electrons.

In the analysis we first selected events with showers. Identification of soft δ–rays is done in the remaining sample. In a four layer system (Fig. 14) we can compute $t_{M1} = (t_A + 2t_B + t_C)/2$ and $t_{M2} = (t_B + 2t_C + t_D)/2$. There is a correlation between the two quantities depending on where a δ–ray is produced: a δ–ray produced in plane A or D will affect only t_{M1} or t_{M2}, while a δ–ray produced in plane B or C will affect both of them. This is clear in Fig. 15 where t_{M1} is plotted against t_{M2}. The data points are distributed along four equally spaced lines showing that most of the δ–rays produced are contained in a single cell. The previous argument does not hold in presence of δ–rays crossing more than one cell. The very good time resolution allows identification if $t_M \geq 4\sigma = 7.5$ ns (equivalent to $\sim$800 μm two track separation) off the peak center. The data

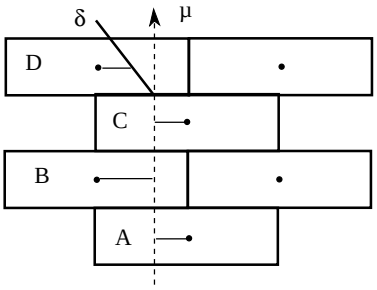

Figure 14: The presence of a δ-electron in one layer leads to a wrong mean timer measurement.

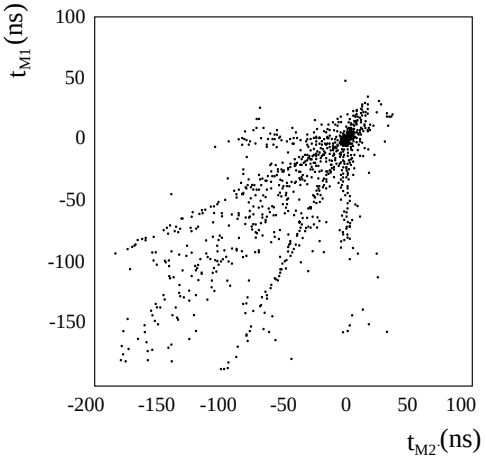

Figure 15: Correlation between the two mean timer measurements obtained from the 4-layer DTBX. Points at the origin represent undisturbed muon tracks. The four lines are an indication for tracks disturbed in only one of the four layers.

p (GeV/c)	δ–rays per cell	showers
100	5.5 ± 0.2	$5.3 \pm 0.3 \pm 0.5$
200	5.5 ± 0.2	$6.7 \pm 0.4 \pm 0.5$
300	6.0 ± 0.2	$7.7 \pm 0.3 \pm 0.5$

Table 5: Fraction (%) of δ–rays and electromagnetic showers. The fraction of δ–rays is computed per cell of 2 cm drift space and at $d > 800$ μm distance from the muon position in the drift direction. The second error is systematic and accounts for corrections applied.

for showers and soft δ–ray production are summarized in Table 5. Only a small fraction ($\sim$20%) of δ–ray events was also seen in more than one layer. The δ–ray production is constant in the investigated muon momentum range, while the shower probability is slowly rising with energy. Corrections for acceptance, detection efficiency and double beam tracks ($\sim$2%) in coincidence in the same event, identified as parallel tracks, were applied to get the right estimation of the rates. The corresponding systematic error is quoted as second error in Table 5.

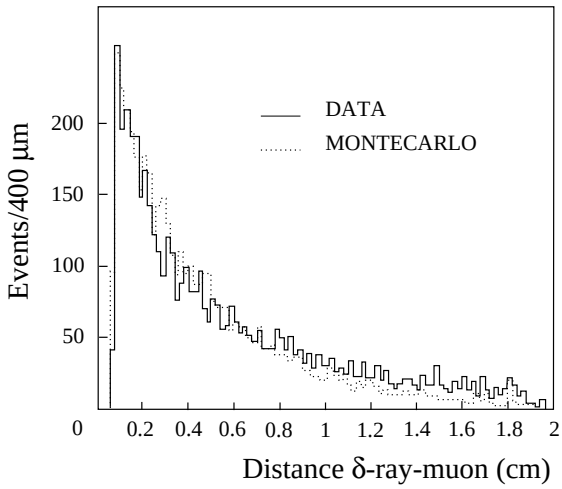

Figure 16: Distribution of the distance between the 'spoiled' hit and the muon track, as obtained from mean timing measurement in the DTBX and from simulation.

The fact that the identification of the δ–ray is obtained from the time information allows to compute the distance of the produced electron from the incoming muon along the shortest drift path to the anode wire. The distribution of this distance is shown in Fig. 16.

2.6 Electromagnetic secondaries in Resistive Plate Chamber

The Resistive Plate Chamber (RPC) is a thin-gap gaseous detector operated in streamer mode which uses a constant and uniform electric field produced by two parallel electrode plates of high bulk resistivity [17]. Its good time response makes it suitable for the first level muon trigger.
The distribution of the charge induced on RPC strips [20] shows a full width at half maximum of about 1 cm, for a 2 mm gas gap at a few mm distance from the pick up electrode. Thus the space resolution is defined by the strip size if this is larger than about 1 cm.
The size of strip clusters as a function of the muon momentum was studied with RPCs of 2×2 m^2 segmented in strips of 3 cm width. The RPCs were operated in discharge mode with a gas amplification of about 10^8 and with digital read out of the charge induced on the strips. We used eight RPCs installed along the beam line in the RD5 spectrometer [21]: four were placed at about 70 cm distance from a 10 interaction lengths absorber, two in narrow gaps in the absorber magnet and the last two at the center of this magnet. Events with hits in at least 4 RPC planes were selected. Signals from adjacent strips were grouped in clusters and then tracks were defined by a least square fit using the centers of the clusters.
The distribution of the number of strips per cluster is shown in Fig. 17 for muon momenta of 100, 200 and 300 GeV/c. A significant broadening of the cluster size with increasing muon momentum is observed and the effect depends on the distance of the RPC from dense absorbers. In Fig. 17 the open dots refer to the two RPCs placed in the gaps of the absorber magnet just behind a 60 cm thick iron wall. The full dots refer to the first two RPCs placed behind the tracking calorimeter, at 70 cm distance from it.

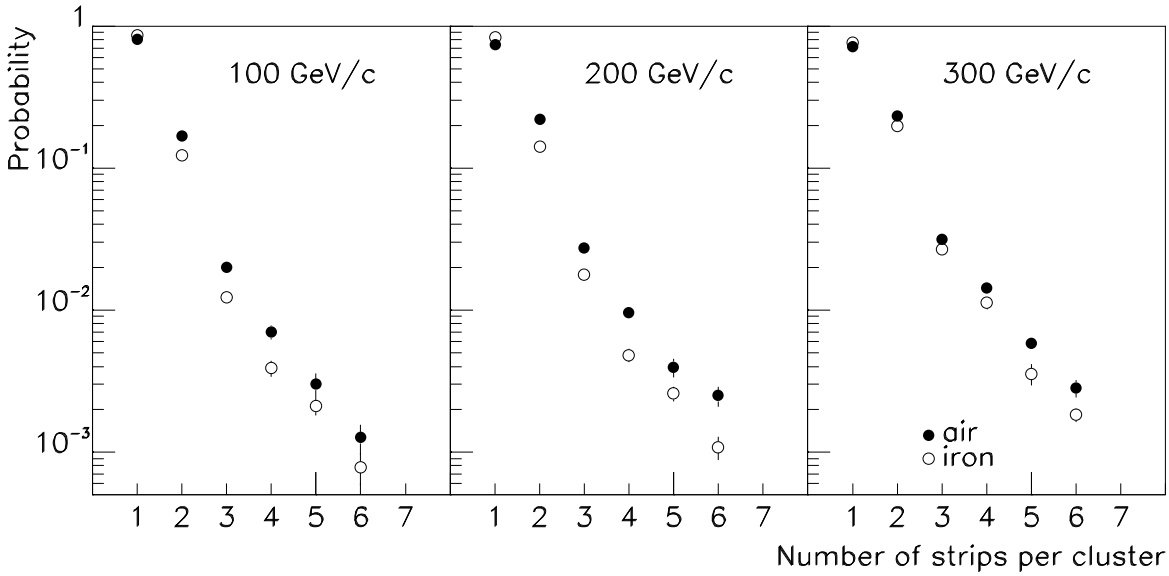

Figure 17: Cluster size distribution for different muon energies. Open dots: RPC placed immediately behind the iron absorber; full dots: RPC placed 70 cm downstream from the absorber. The strip width is 3 cm.

The effect of the increasing probability of producing e.m. secondaries contributes to widen the cluster size distribution and is clearly different for the two RPC positions: it is reduced for the RPC close to the iron absorber. However the average size of clusters is slightly affected varying from 1.17 to 1.38 strips. The rms width of the residuals from the track fit is about 7 mm and is independent of the muon momentum. Thus the selectivity of a tracking muon first level trigger based on RPCs segmented in strips of few cm width and a simple cluster algorithm, like that used in the trigger processor of ref. [22], will not be much affected by the effect of e.m. secondaries.

3 Further predictions for the LHC environment

The simulation results presented in the preceding sections did take into account most of the details of the individual detector used. In order to make further predictions, we have performed a simulation using the GEANT program [9] with a simplified geometry: muons traverse at normal incidence a 60 cm thick iron block and several idealized detector planes placed at different distances from the absorber. These detector planes are assumed to have full detection efficiency, no mass and no limits on the resolution or on the capability to distinguish between two hits. Charged particles and photons have been traced in the simulation program until their energy is as low as 0.1 MeV and their position in the detector planes have been recorded. This simplified simulation was done for the detector sizes and positions used in our measurements and reproduced the observed rates within 10%.

Being confident on the reliability of the simulation for a simplified geometry, we can use it to make predictions of the effect of additional particles on the identification of the muon hit in the LHC experimental conditions. We have studied three different cases: without magnetic field, with a magnetic field of 0.6 T in air (downstream of the absorber; magnetic field orthogonal to the muon track), and with a magnetic field of 1.8 T only in the iron. The last two situations are characteristic for the muon systems of the planned LHC detectors [4, 5]. No significant difference is found whether the iron absorber is magnetized or not: the δ–electrons reaching the detectors are those produced in the last few millimeters of the absorber and thus are not deflected by the magnetic field; the

effect of multiple Coulomb scattering is more important than the bending power for those produced further upstream in the absorber.

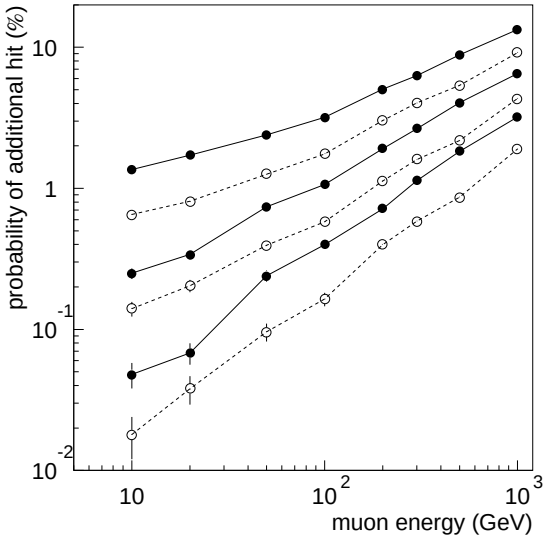

Figure 18: Simulation: probability of having a muon hit spoiled by the presence of at least one additional electron hit within a two hit resolution of 15, 5 and 2 mm (top to bottom). The detector is at 15 cm from the absorber. Solid lines are for magnetized iron; dashed lines for 0.6 T downstream of the absorber.

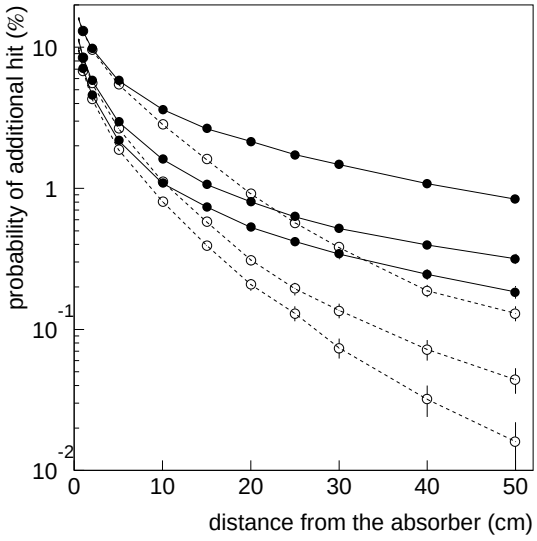

Figure 19: Probability of having a spoiled muon hit versus the distance from the absorber for a two hit resolution of 5 mm. The muon momentum is 300, 100 and 50 GeV/c (top to bottom). Solid lines are for magnetized iron; dashed lines for 0.6 T downstream the absorber.

According to the simulation, the probability for a muon to be accompanied by at least one additional electron behind the absorber raises from 16% at 50 GeV to 37% at 1 TeV. The effect of the spurious hits on the effective spatial resolution will be, at the end, strongly dependent on the detector response.

One way to improve the situation is to use detectors with rather good multihit capability: the hits due to the muon and to the electron(s) can be detected individually and then the two particles identified, provided there are no reconstruction ambiguities. In this case the crucial parameter is the two hit resolution of the detector. Figure 18 shows, for a detector located at 15 cm distance from the absorber, the fraction of events with at least one additional hit separated from the muon hit by a distance smaller than the two hit resolution: in the case of a drift chamber this number has to be divided by a factor of 2, assuming that if the muon hit is closer to the anode wire than the electron hit its drift time measurement is not disturbed. The fraction of spoiled muons can be strongly reduced by exploiting a two hit resolution of 5 mm or better.

If a magnetic field is applied in the region downstream of the absorber slow electrons cannot reach the detector placed at some distance, while those with higher energy emerging parallel to the muon track are swept away from it. The results of the simulation for a magnetic field of 0.6 T are also shown in Fig. 18.

The fraction of events with additional hits within the two hit resolution of a detector decreases also when the detector is moved further away from the absorber: this effect is shown in Fig. 19 for different muon momenta, both with and without a magnetic field. The detectors should not be placed too close to the iron wall; good results can be obtained already for distances of about 15 cm. For a given muon spectrometer magnet it is also useful to exploit the choice of the wall thickness of the muon chamber to minimize the disturbing effect of any additional hit(s) nearby the muon hit. If the chambers can be placed in a magnetic field and at sizeable distances from the massive

muon filter (as e.g. in [5]) the tracks from e.m. secondaries will be well separated from the muon track. The use of nearly massless muon chambers will avoid the production of secondaries inside the chamber.
In an opposite scenario, the muon chambers are interspaced with thick layers of magnetized iron to form a compact spectrometer (as e.g. in [4]) in which high energy secondaries affecting one muon chamber are safely absorbed and cannot reach the next one. The distance between iron and chambers is naturally kept small in such design, and there is interest to use the muon chamber material to absorb the softest secondaries, or to scatter them considerably. This basically reduces the number of disturbing hits and/or helps to recognize their presence.
A chamber with 6 layers and 14 mm wide cells, and a pulse length of 100 ns or larger was simulated with massive (aluminium) and massless (air) walls about 1 cm thick between each gas layer. Three different situations were compared: a gap of 0.8 cm between iron and chamber, a gap of 13 cm, and no iron in front of the chamber. It turns out that in the presence of an iron absorber the total number of electrons per layer in an aluminium chamber is about half the number in a massless chamber. The amount of electrons originating in the iron decreases with increasing depth in the massive chamber, but not in the massless one. To show how often the reconstructed track is affected in these extreme situations, Table 6 gives the fraction of tracks deviating significantly from the generated muon track (using the matching criterion which is described in the following section). It evidences that for a massive (massless) spectrometer the use of a correspondingly massive (massless) chamber is advantageous. It is obvious that since the response to e.m. secondaries is not the only criterion for the actual chamber choice in the detector, a mix of the two situations is more likely to occur.

chamber material	between chamber and iron		*without* iron
	gap of 0.8 cm	gap of 13 cm	
aluminium	4.7	3.5	2.2
air	7.0	4.2	0.16

Table 6: Fraction of tracks (%) not matching well the real muon track for a WLDC-like geometry, as simulated for a massive and a nearly massless chamber.

4 Impact on muon measurement and trigger

In order to measure the impact of the production of e.m. secondaries on the reconstructed track position and angle, an external definition of the muon track is required, to compare it with the reconstructed track. Here the information from the 'first muon station' in RD5 is used as an external reference for the WLDC chamber. A muon track from the first muon station is required to have a $\chi^2/d.o.f.$ better than 3, to be triggered by the 2×2 cm^2 trigger counter and to be located within 2 cm from the beam axis at the first muon station. Such tracks are taken as reference for comparison with the track reconstructed in the WLDC located about 60 cm upstream.
To quantify the deviation of a track measured in the WLDC from the reference track in position (Δx) or in angle ($\Delta\theta$) a variable $R = \sqrt{(\Delta x/4\sigma_x)^2 + (\Delta\theta/4\sigma_\theta)^2}$ is defined. A value of $R < 1$, i.e. a deviation below about 2.8σ is required for 'good matching'. Figure 20 shows the distribution of this variable R for the different event classes determined by the number of large signed residua. Table 7 gives the fraction of non-matching tracks for different data samples. Since the reference track also has errors and had to be extrapolated over about 60 cm, the matching error expected from this measurement is larger for the track position than for the track angle. Therefore, the matching criterion will reject mainly angular mismatches. The number of non-matching tracks is correlated to the number of bad hits. This demonstrates that large residua in the (local) track reconstruction indicate well the matching quality.

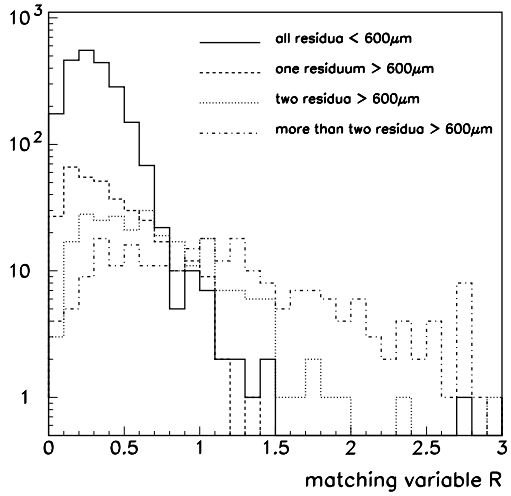

Figure 20: Muons of 200 GeV measured in the WLDC and compared with an external track measurement. Distribution of the matching variable R measured for different event classes. For 'good matching' we require $R < 1$. Since here the reference track had to be extrapolated over a long path, a large R reflects mainly angular mismatches.

energy of muons	amount of tracks with $R > 1$ quality of reconstructed track				weighted sum
	all residua $< 3\sigma$	one residuum $\geq 3\sigma$	two residua $\geq 3\sigma$	more than two residua $\geq 3\sigma$	
10 GeV	0.7±0.4	11.7±3.9	13.2±5.0	28.3±7.8	5.1±0.9
30 GeV	0.4±0.2	2.5±1.3	13.1±3.2	51.3±6.6	5.5±0.6
50 GeV	0.6±0.2	2.9±1.3	15.4±3.6	41.0±5.9	5.1±0.6
100 GeV	0.5±0.3	3.8±2.2	14.8±4.9	47.6±8.7	5.7±0.5
200 GeV	0.5±0.2	1.2±0.6	15.3±2.4	49.6±4.4	5.9±0.4

Table 7: Fraction (%) of tracks in WLDC not matching the external muon track. The matching criterion is $R < 1$. Good tracks (all residua $< 3\sigma$) do always match the external measurement.

For the total sample, about 5 to 6% of the tracks fail the matching criterion (Tab. 7, last column). This amount depends also on the reconstruction parameters. For example, when narrowing the search path for hits from 5 to 2 mm, 0.2% of the tracks are not reconstructed, but the fraction of reconstructed tracks 'not matching' (i.e. with $R > 1$) is reduced from 6% to 2%, thus featuring an obvious gain.
The actual deviation in angle and position of the reconstructed track segment from the original muon was studied with a simulation based on the empirical data. For this study, 8 'muon hits' were generated in the WLDC along a straight line. The probability that a hit is spoiled was determined according to the probabilities in Tab. 4. The distance (>600 μm) of the 'spoiled' hits from the ideal track was distributed according to Fig. 10. This space coordinate is translated into a drift time taking into account the effects of cell geometry, primary ionization and diffusion in the drift gas, as simulated with the GARFIELD [19] program, and then parametrized. Since no further errors were accounted for nor were inclined tracks generated, the resulting single hit resolution of 160 μm is better than the 187 μm measured.
When all hits are used in the reconstruction, the errors of the track segment are $\sigma_x(track) = 52$ μm in position and $\sigma_\theta(track) = 0.74$ mr in angle. About 17.2% of the events do not fulfil the matching criterion $R < 1$, as shown in Fig. 21. Note that here the ideal muon track is taken as reference and does not contribute to the errors; therefore the cut R <1 is more stringent.
To reduce the impact of electromagnetic secondaries, spoiled hits were removed in the following way. The hit with the largest residuum is removed if the residuum is larger than 350 μm, and the track reconstruction is redone. This procedure is iterated until all residua are below 350 μm, or only 4 hits are left. (Varying this geometrical cut over a wide range, it appears that the resulting track errors are lowest for 350 μm.) The track errors, for the whole sample, are slightly reduced to $\sigma_x(track) = 45$ μm and $\sigma_\theta(track)$ =0.65 mr, and only 4.1% of the tracks fail the matching criterion (Fig. 21). This means that the number of 'bad matching' tracks is now 4.2 times smaller. The significant improvement in track quality is mainly related to the events affected by e.m. secondaries. This is best evidenced by looking at the events where an e.m. secondary is known to be present (Fig. 22).
Finally, the presence of e.m. secondaries is not expected to have an impact on the 1^{st} level (hardware) muon trigger in the case of a massive muon spectrometer. For triggering on low energy muons, the logical cell width of the detector will be wider than the apparent shift due to e.m. secondaries. Also when triggering on high energy muons there will be no loss of signal, as long as 4 stations are available and 3 out of the 4 stations are required for the trigger. On the other hand, sometimes an e.m. secondary may cause the muon track to appear less bent, simulating a higher momentum and thus increasing the trigger rate.

5 Conclusions

Production of muon induced e.m. secondaries is sizeable at LHC energies. The presence of e.m. secondaries is likely to corrupt the muon measurement. A very demanding track reconstruction and track matching between tracker and muon detector cannot tolerate a disturbed muon measurement, especially while searching for extremely rare events.
Details of the simulation of the production of secondaries, down to very low electron energies, are well confirmed by highest resolution data obtained with the silicon detector. We have studied the effect of e.m. secondaries on the detection of muons with energies up to 300 GeV in a test beam, using various detector technologies. It was shown how the presence of e.m. secondaries is recognized in each multi-layer chamber forming a muon 'station'. All detector types succeed in identifying the track segment and even the individual cell affected by such a secondary. Affected track segments can thus be reliably removed from the reconstruction.
In a large fraction of the cases, only 1–2 layers of a station are affected. Instead of discarding the whole track segment in the station, one can remove the affected hit(s) only. Simulation demonstrates that by removing the 'spoiled' hit and refitting the track, about 75% of the tracks originally failing

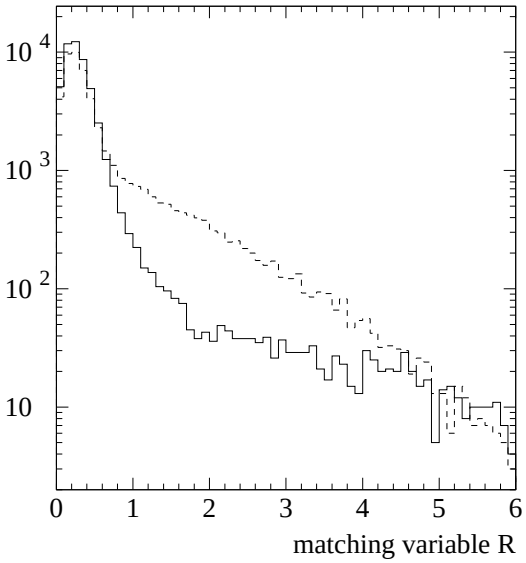

Figure 21: Distribution of the matching variable R using all hits (dashed line) and after removal of hit(s) outside 350 μm and refitting the track (solid line) for simulated events in an 8-layer WLDC. The fraction of tracks having R above 1 is reduced from 17.2% to 4.1%. Here R is calculated w.r.t. the (known) true muon track.

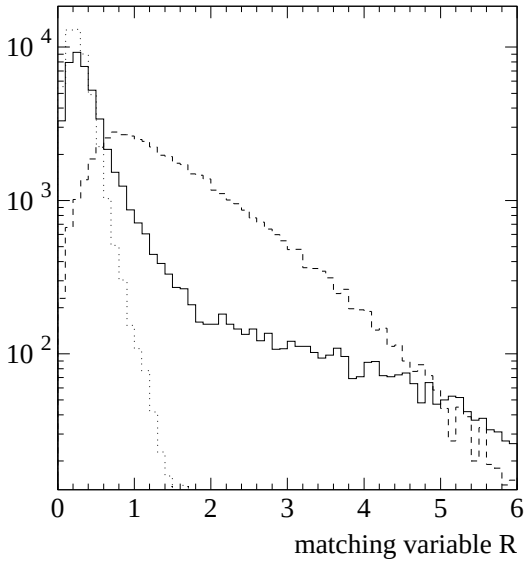

Figure 22: Distribution of the matching variable R for those simulated events having at least one e.m. secondary, using all hits (dashed line) and after removal of hits outside 350 μm (solid line). The fraction of tracks with R above 1 is reduced from 63.9% to 15.2%. As a reference, the distribution for undisturbed muons (no e.m. secondaries; dotted line) features 0.6% of the events with R above 1. The three curves are normalized to the same area.

the matching criterion because of the presence of e.m. secondaries can be recovered. This method is powerful and should therefore be further exploited. Matching measurements confirm that a reconstruction including the affected layers leads to most of the mismatches.
In the case of an iron spectrometer the presence of a thick absorber ($\sim$30 X_0) between measuring stations ensures that an e.m. shower can affect at most one muon station. The number of disturbing e.m. secondaries can be further reduced by using massive muon chambers able to scatter and/or absorb more such secondaries than they produce. In addition, the number of disturbing e.m. secondaries can be significantly reduced by having some empty space between the last absorber and the muon chambers. This is especially useful in the case of an air spectrometer.
The detectors studied are able to recognize a muon hit spoiled by an overlapping electron hit. This means that in a multilayer chamber the intrinsic single hit resolution alone can discriminate against e.m. secondaries and that there is no need for a demanding two-track resolution. In case of a muon chamber with few layers our studies indicate that a good multihit capability reduces the effects of e.m. secondaries.
The impact of e.m. secondaries on the hardware trigger is expected to be small.

6 Acknowledgments

For their support in the preparation and during the actual runs we thank S. Lazic, D. Peach, P. Petiot, J. Pothier, B. Powell, A. Tusi and G. Waurick.

7 References

References

[1] M. Della Negra *et al.*, CERN/DRDC/90-36, DRDC/P7 (1990).

[2] RD5 Collaboration, M. Aalste *et al.*, Z. Phys. **C60** (1993) 1.

[3] RD5 Collaboration, H. Faissner *et al.*, CERN/DRDC/93-49 (1994).

[4] Letter of Intent, CMS Collaboration, CERN/LHCC 92-3 (1992).

[5] Letter of Intent, ATLAS Collaboration, CERN/LHCC 92-4 (1992).

[6] See e.g. W. Lohmann, R. Kopp and R. Voss, Yellow Report CERN 85-03, 21 march 1985.

[7] Aachen-Padova Collaboration, private communication. The detector, used until 1975, consisted of a 7 m long and $>$20 X_0 deep array of 2×2 m^2 optical spark chambers with a granularity of about 0.1 X_0.

[8] W.K. Sakumoto *et al.*, Phys. Rev. **D45** (1992) 3042.

[9] R. Brun *et al.*, GEANT simulation package, CERN Program Library.

[10] RD5 Collaboration, A. Böhrer *et al.*, CERN/DRDC/91-53 (1992).

[11] H. van der Graaf *et al.*, Nucl. Instr. and Meth. **A307** (1991) 220.

[12] F. Bakker *et al.*, Nucl. Instr. and Meth. **A330** (1993) 44.

[13] Dubna Group, in Milestones Report, CMS Collaboration, CERN/LHCC 93-48, p. 70.

[14] G. Bencze *et al.*, "Position and Timing Resolution of Interpolating Cathode Strip Chambers in a Test Beam", report RD5 TN/94-03, submitted to Nucl. Instr. and Meth.

[15] H. Faissner *et al.*, Nucl. Instr. and Meth. **A330** (1993) 76;
H. Faissner *et al.*, "Performance of a Wall-Less Drift Chamber for Muon Detection", submitted to Nucl. Instr. and Meth. **A**.

[16] The single hit resolution assumed in the simulation was 250 μm and the data turned out to have 200 μm; therefore there are somewhat fewer events with hits outside 3σ in the simulation.

[17] R. Santonico and R. Cardarelli, Nucl. Instr. and Meth. **A187** (1981) 377;
R. Cardarelli *et al.*, Nucl. Instr. and Meth. **A263** (1988) 20.

[18] F. Gasparini *et al.*, Nucl. Instr. and Meth. **A336** (1993) 91.

[19] R. Veenhof, GARFIELD drift chamber simulation package, CERN Program Library.

[20] L. Pontecorvo: Proceedings of the II International Workshop on Resistive Plate Chambers in Particle Physics and Astrophysics, Scientifica Acta **3** (1993) 145;
F. Ceradini *et al.*, "Measurement of the hit distribution in Resistive Plate Chambers with a digital read out of the charge induced on strips", Internal note 990, Dipartimento di Física, Università di Roma "La Sapienza", 9.12.1991.

[21] Gy.L. Bencze *et al.*, Nucl. Instr. and Meth. **A340** (1994) 466.

[22] E. Petrolo and S. Veneziano: Nucl. Instr. and Meth. **A344** (1994) 194.

Remark to the technical office:

This text was written with LaTeX. The corresponding file is available on request from:

H. Reithler, Phys. Institut IIIA, RWTH Aachen, A. Sommerfeld Str. D-52056 Aachen

E-mail: reithler@acv3a1.hep.rwth-aachen.de
Tel. +49-241-807330 or 807325, Fax +49-241-8888189.